



Research paper

Optimization of heavy haul railway tunnel lining based on ultimate bearing capacity

Wei Han¹, Taoli Xiao², Duanwen Shi³, Yupeng Wang⁴

Abstract: The optimization process of design parameters for composite lining of heavy haul railway tunnel is a key problem to be solved in tunnel engineering design. In order to put forward a better design scheme of composite lining for heavy haul railway tunnel, combined with field measurement and numerical simulation, the optimal working condition design is carried out by changing the thickness of shotcrete layer, the type of grid steel frame and the thickness of secondary lining. The influence of the above design parameters on the stress state of the composite lining is analyzed to obtain the optimal design parameters. Finally, the safety performance of the optimized lining is evaluated by the ultimate bearing capacity curve of the secondary lining section. The research shows that: 1) The optimal design parameters of the composite lining of the tunnel are the thickness of the shotcrete layer of 25 cm, the type of the grid steel frame of H180, the thickness of the secondary lining arch waist and the side wall of 40 cm and 35 cm respectively; 2) Different from the single-track heavy haul railway tunnel, the displacement value of the vault settlement of the double-track heavy haul railway tunnel is significantly greater than that of the inner convergence. Increasing the thickness of the shotcrete layer and changing the type of the grid steel frame have better effects on reducing the vault settlement, and have little effect on the inner convergence.

Keywords: safety factor of bending resistance, safety of lining structure, tunnel engineering, lining optimization, ultimate bearing capacity

¹MSc., Eng., Fujian Forestry Vocational and Technical College, Department of Traffic Engineering, Nanping, 353000, China, e-mail: hanwei202203@163.com, ORCID: 0000-0002-2944-8525

²Prof., PhD., DSc., Yangtze University, School of Urban Construction, Jingzhou, 434000, China, e-mail: xtl20220507@163.com, ORCID: 0000-0001-6796-8268

³MSc., Eng., China Railway Fourth Survey and Design Institute Group Co.,Ltd, tunnel engineering, Wuhan, 430000, China, e-mail: 1904702503@qq.com, ORCID: 0000-0002-3874-1838

⁴MSc., Eng., Fujian Forestry Vocational and Technical College, Department of Traffic Engineering, Nanping, 353000, China, e-mail: 2804210133@qq.com, ORCID: 0000-0002-4859-1386

1. Introduction

Research on the stress state of composite lining is the foundation of tunnel engineering design. In the actual structure design of composite lining, engineering analogy method and theoretical analysis are usually used to determine the design parameters of secondary lining at home and abroad. Sauer et al. [1] used the section $M-N$ curve to determine whether the bearing capacity of the lining section meets the load effect. Kaper et al. [2] analyzed the application of steel fiber reinforced concrete (SFRC) segment in the durability design of lining structure combined with practical engineering. Qiu et al. [3] studied the influence of section size and material strength on the ultimate bearing capacity of section based on local bending test. Mai et al [4] studied the $M-N$ curve of reinforced concrete square column and circular column, and concluded that the $M-N$ curve will be larger when the spacing of reinforcement is low. Ma et al. [5] established the coupling calculation model of tunnel and surrounding rock by finite difference method, and studied the fatigue life characteristics of concrete structure at the bottom of railway tunnel. Pengfei et al. [6] utilized three-dimensional numerical software to establish the dynamic analysis program of tunnel. Through the analysis of stratum deformation, support force and plastic zone distribution, the optimized tunnel construction scheme is obtained. Vanuvamal and Jaya [7] conducted a comparative study on support design methods such as Terzhagi's load theory and quantitative methods of Rock mass quality, Rock mass rating of Bieniawski and PLAXIS-2D numerical modeling. The results show that the final supporting measures such as shotcrete, thickness, bolt, length, frequency and steel support are better, which provides specific supporting measures for a tunnel. Ghaffari and Mahdevari [8] utilized three-dimensional numerical simulation method to study the influence of tunnel diameter, thickness and surrounding rock geomechanical parameters on tunnel displacement profile. Yertutanol et al. [9] studied that in the stress redistribution caused by tunnel excavation disturbance, neither rock nor lining reached yield strength. In view of the large deformation often occurred during tunnel construction, Gao et al. [10] proposed an optimized support scheme to strengthen the stiffness and strength of the initial support and weaken the bolt. The feasibility of the scheme was evaluated by numerical simulation and field monitoring. Jiang et al. [11] studied the deformation mechanism and stability of long-span highway tunnel, compared different construction schemes, and gave the optimal construction scheme. Choi and Shin [12] utilized three-dimensional finite difference software to simulate the actual situation and proposes the optimal support scheme. Rahim et al. [13] studied the rock response of shallow double-hole excavation by numerical analysis. Qu et al. [14] studied the initial release load law of steel arch support and the change law of bearing capacity of two support structures with time, and gave the applicable conditions of steel arch and steel grid. Wang et al. [15] conducted in-situ control test on the internal displacement of surrounding rock by using multi-point extensometer before tunnel excavation. Zeng et al. [16] proposed the analytical solution of tunnel lining pressure caused by tunnel section distribution. Zhang and Qi [17] proposed intelligent construction measurement method to shorten construction period and reduce engineering risk. Combined with 3D Finite element software, Leonardi et al. [18] described the tunnel response considering structural safety and gave preventive measures.

At present, the lining structure design of tunnel engineering in China is mainly based on the engineering analogy method guided by experience and lacks reliable theoretical guidance, which leads to the conservative design of tunnel lining. For example, the excessive thickness of the secondary lining will increase the self-weight of the lining itself, resulting in longer cracks. However, there is a lack of systematic research on this in China and abroad.

In this paper, a tunnel along the Menghua railway is taken as the engineering background. Referring to the research results of tunnel composite lining structure at home and abroad, on the basis of the original tunnel composite lining, the actual engineering field monitoring and application are carried out by changing the thickness of the spray layer and the height of the grid steel frame. The original design and optimization design conditions are compared, and the internal force and bending moment of the composite lining are analyzed by numerical calculation. Combined with the ultimate bearing capacity curve of the lining section, the calculation results are evaluated, and the optimal design parameters of the lining of the double-track railway tunnel under the condition of grade IV surrounding rock are obtained, in order to provide reference for the lining design of similar projects.

2. Research program

2.1. Project profile

The proportion of tunnels along the Menghua Railway is as high as 28.2%. The tunnel passes through loess, sandy layer and granite, and there are adverse geological conditions such as water-rich faults, high ground stress and weak surrounding rock. In order to study the stress of composite lining of loess double-track tunnel under the condition of grade IV surrounding rock, Guoqi tunnel was selected to carry out experimental research and numerical simulation. As one of the representative tunnels, Guoqi tunnel is initially supported by shotcrete, as shown in Fig. 1. The process geological conditions of tunnel crossing are complex, the construction is difficult and the risk is high. Fig. 2 shows the original lining section design.



Fig. 1. Tunnel site test construction drawing

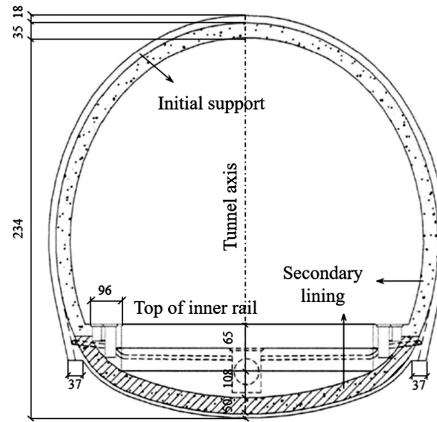


Fig. 2. Original design for lining section

2.2. Design parameter

On the basis of the original lining section design, two new Cases were designed by thickening the spray layer, changing the model of the grid steel frame and reducing the thickness of the secondary lining. The thickness of the spray layer was increased by 3 cm in Case 2 and 3, and the H180 grid steel frame was used. On the basis of the original design, the thickness of the arch wall and the inverted arch was reduced by 10 cm and 5 cm in Case 2. Working condition 3 reduced the thickness of arch wall and inverted arch by 5 cm and 10 cm respectively on the basis of the original design. The specific parameters of each working condition are shown in Table 1.

Table 1. Support parameters under test conditions

Case	Initial support				Secondary lining	
	C25 shotcrete		Steel truss		Arch wall	Inverted arch
	Site	Thickness (cm)	Site	Model/spacing	Thickness (cm)	Thickness (cm)
Case 1	whole ring	22	whole ring	H150/1.0 m	45	50
Case 2	whole ring	25	whole ring	H180/1.0 m	35	45
Case 3	whole ring	25	whole ring	H180/1.0 m	40	35

Note: The inverted arch is reinforced concrete

2.3. Field monitoring

In order to study the stress change of tunnel and the stress characteristics of supporting deformation during construction. Internal force of tunnel lining is monitored during tunnel construction.

The internal space deformation and vault settlement of the tunnel can directly reflect the change of the stress state of the surrounding rock. Through the deformation of the surrounding rock of the tunnel, the stability of the tunnel after the support construction can be effectively judged, and the field design and construction can be guided. The site measuring point layout is shown in Fig. 3. The layout of measuring points for tunnel deformation and vault settlement is shown in Fig. 3a; the stress of shotcrete is monitored by the embedded concrete strain gauge for the strain of the initial concrete, and then the corresponding stress is obtained, with 12 measuring points arranged in each section and 2 measuring points inside and outside, as shown in Fig. 3b. The internal force of the grille steel frame is monitored by the steel frame stress meter, 12 measuring points are arranged in each section, and 2 measuring points are inside and outside, as shown in Fig. 3c.

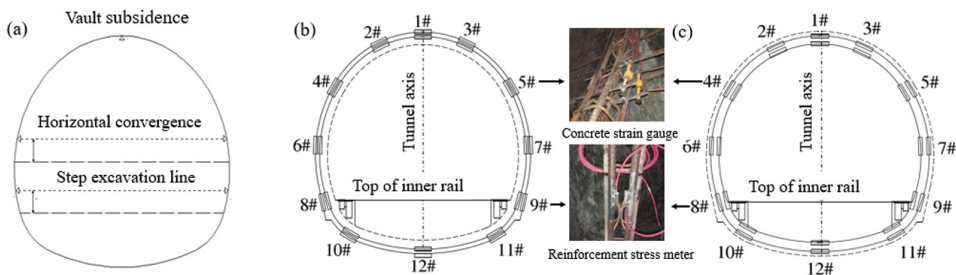


Fig. 3. Site monitoring measuring point layout (a) displacement measuring point; (b) Initial support measuring points; (c) Secondary lining measuring points

2.4. Numerical calculation

In order to further reveal the influence of lateral pressure coefficient on the internal force of tunnel lining, the variation characteristics of support internal force with construction process are analyzed, and the construction project of tunnel is numerically simulated.

The size of the model is $80 \times 120 \times 30$ m. In the model, the surrounding rock, the initial support and the secondary lining are simulated by solid elements, the surrounding rock is modeled by Mohr-Coulomb constitutive model, and the initial support and the secondary lining are modeled by elastic constitutive model. The buried depth of the tunnel is 80 m. The partial grid of the tunnel is encrypted, the bottom of the grid is fully constrained, and the lateral constraint is applied. The numerical calculation model is shown in Fig. 4. In the process of tunnel excavation, the release coefficient of in-situ stress is used to simulate. Through the LDF module of the software, namely, each step of excavation releases 60% of the in-situ stress without excavation, and 40% of the in-situ stress is released during

support, and the step is gradually excavated and supported. Through numerical calculation, the stress of composite lining under three Cases is finally obtained and converted into the internal force of composite lining section.

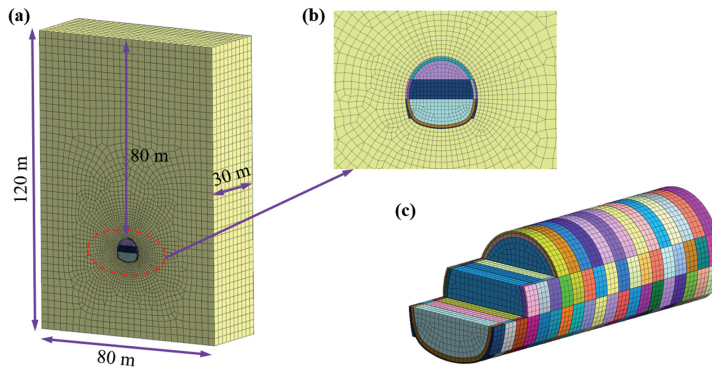


Fig. 4. Calculation model grid: (a) overall model; (b) local model; (c) tunnel excavation model

On the basis of the field test and related geological exploration reports, the physical and mechanical parameters of surrounding rock are determined by RMR method, and the calculation parameters of support are determined according to the elastic modulus of shotcrete and steel frame. The calculation parameters of tunnel surrounding rock and support are shown in Table 2.

Table 2. Physical parameters of surrounding rock and support

Project	Elastic modulus (GPa)	Poisson ratio	Angle of internal friction (°)	Cohesion (MPa)
Surrounding rock	2.8	0.33	30	2
Initial support	34.79 (34.84)	0.2		
Secondary lining	33	0.2		

Note: The elastic modulus of the initial support is equivalent bending elastic modulus; parameters for new conditions 2 and 3 in parentheses

3. Result analysis

3.1. Analysis of convergence of initial support and vault settlement

As the research object of this paper is deep buried tunnel, the deformation of the initial support of the tunnel should be analyzed. Fig. 5, 6 and 7 show the displacement diagram of the initial support when the excavation is completed under three Cases. It can be seen from

Fig. 5, 6 and 7 that the decline value of the initial support vault is significantly greater than the horizontal displacement change value on both sides of the arch waist. The reason for this phenomenon is that the tunnel in this paper is deeply buried and the size distribution of the tunnel section of the double-track tunnel is relatively uniform. Therefore, the influence of tunnel excavation on the vault is significantly greater than that on the arch waist.

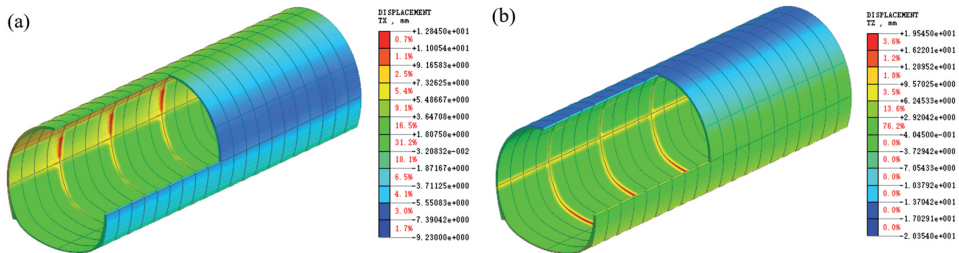


Fig. 5. Initial support displacement change chart (Case 1): (a) x-direction; (b) z-direction

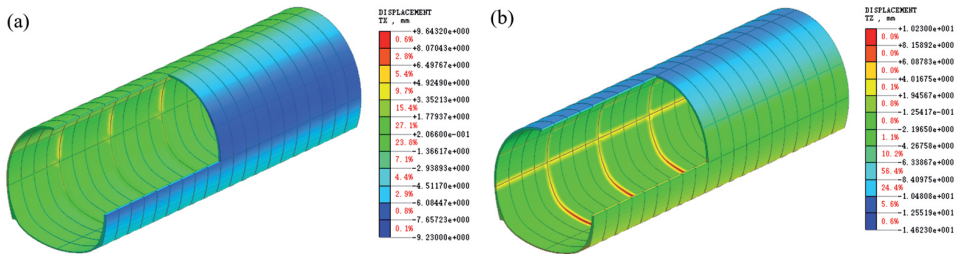


Fig. 6. Initial support displacement change chart (Case 2): (a) x-direction; (b) z-direction

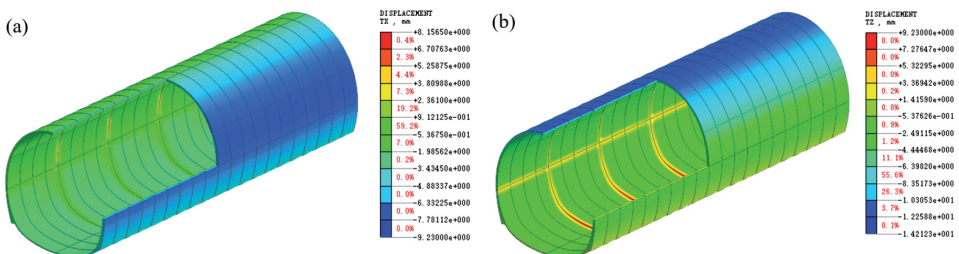


Fig. 7. Initial support displacement change chart (Case 3): (a) x-direction; (b) z-direction

Combined with the field monitoring data and numerical calculation results, the variation curves of the convergence of tunnel internal space and vault settlement with the construction date (construction process) are obtained, as shown in Fig. 8, 9, 10.

It can be seen from Figure 8, 9, 10 that the calculation results of numerical simulation are slightly larger than the measured results. According to the measured results, the conver-

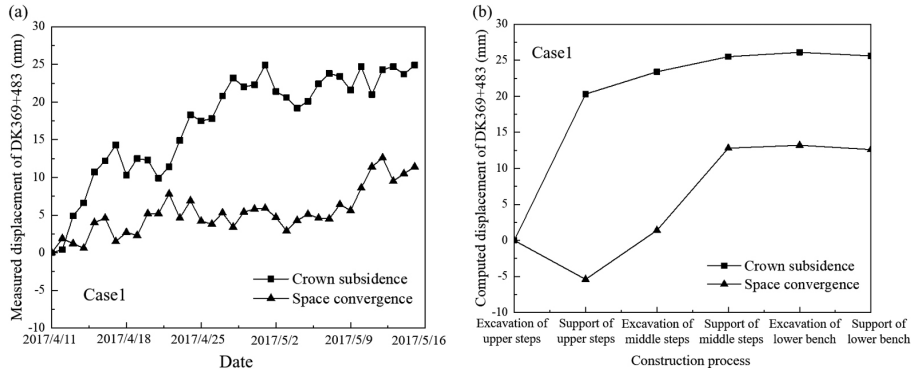


Fig. 8. Curves of inner void convergence and vault settlement versus time or construction process (Case 1): (a) Measured; (b) Computed

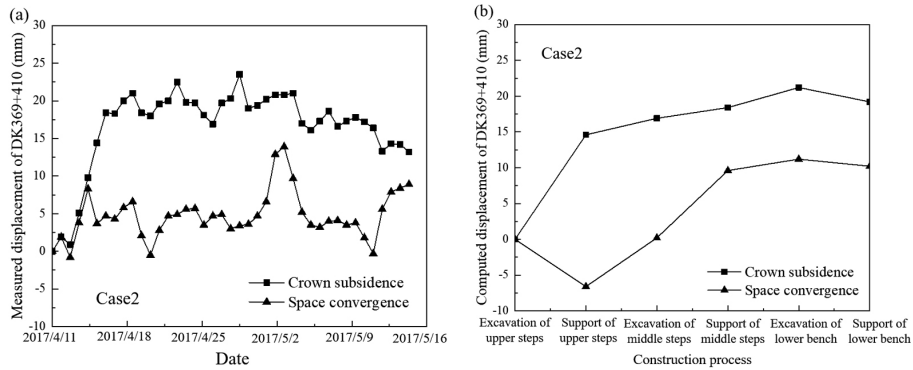


Fig. 9. Curves of inner void convergence and vault settlement versus time or construction process (Case 2): (a) Measured; (b) Computed

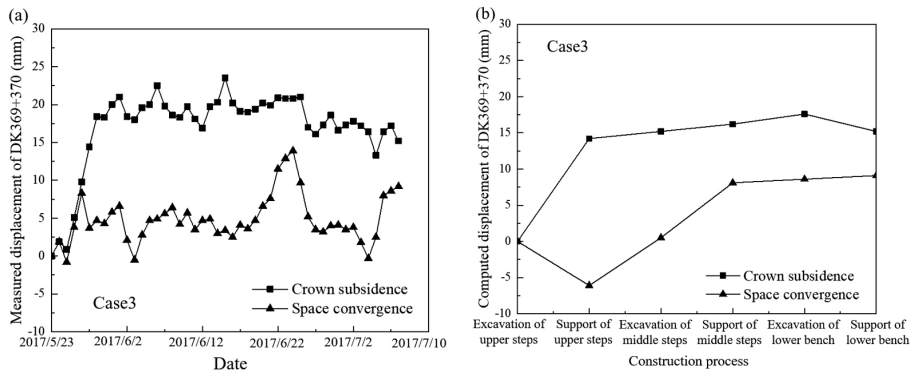


Fig. 10. Curves of inner void convergence and vault settlement versus time or construction process (Case 3): (a) Measured; (b) Computed

gence of the inner space and the settlement of the vault increase gradually with the increase of time. Most of the displacement will generally occur within 2 weeks, and then gradually converge. There is a certain fluctuation in the displacement value. After the completion of the construction, the convergence value of the vault settlement is about 10–25 mm. The internal space convergence displacement is 5–15 mm. In different Cases, after shotcrete thickening, the vault settlement and the convergence deformation of inner space are reduced. The vault settlement value decreases obviously, about 10–15 mm. According to the numerical simulation, the vault settlement of Case 1, 2 and 3 is 20.3 mm, 14.6 mm and 14.2 mm respectively when the excavation and support of the upper bench is completed, and then gradually increases with the excavation steps, and the final convergence values are 25.6 mm, 19.2 mm and 15.2 mm respectively. In case 1, 2 and 3, the convergence of inner space is -5.4 mm, -6.6 mm and -6.1 mm respectively when the upper bench support is completed. The convergence of inner space changes obviously in the process of middle bench excavation and support, which are 12.8 mm, 9.6 mm and 8.1 mm respectively. The final convergence values are 12.6 mm, 10.2 mm and 9.1 mm respectively. Under three conditions, the numerical simulation results of vault settlement and interior convergence are slightly larger than those of monitoring measurement, about 5–10%. Compared with the original decrease of 47% and 39%, the inner space convergence displacement values decreased by 19% and 22%, respectively.

On the basis of the above analysis, it can be concluded that the initial deformation of the tunnel is mainly vault settlement, which indicates that the vertical and horizontal stress of the tunnel in the site selection area is uneven; the effect of increasing the thickness of mixing layer on vault settlement is more obvious than that of inner convergence.

3.2. Internal force analysis of initial support

Combined with field monitoring and numerical analysis, the internal forces of the grid steel frame at the vault (1#), arch shoulder (2# and 3#), arch waist (4# and 5#), side wall (6# and 7#), arch foot (8# and 9#) and inverted arch (10#, 11# and 12#) under three Cases are shown in Fig. 11, 12 and 13.

It can be seen from the Figure 11, 12, 13 show that the axial force (pressure is negative, tension is positive) of the grid steel frame is pressure, and the pressure range is about $-250 \div 0$ kN; the axial force of the grid steel frame is generally characterized by 'large arch, followed by side wall and small inverted arch'. Based on field test, the maximum axial force of the grid steel frame occurs at the side wall (6#) position, which is -247.14 kN. It can be seen from the figure that the axial force of the grid steel frame (the pressure is negative, and the tensile force is positive) is expressed as the pressure, which is about $-250 \div 0$ kN, and the overall distribution characteristics are as follows: 'The arch is large, followed by the side wall, and the inverted arch is small'; according to the field monitoring, the maximum axial force of the grid steel frame appears at the measuring point of the side wall (4#), which is -247.14 kN.

The bending moment of the grid steel frame (the lateral compression and the inner tension are negative) has the difference between the internal and external bending, which

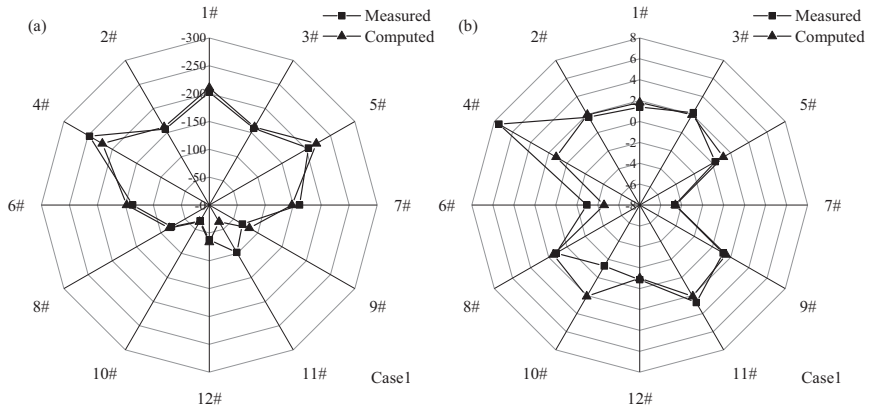


Fig. 11. Internal forces of grille steel frames (case 1): (a)Measured; (b):Computed

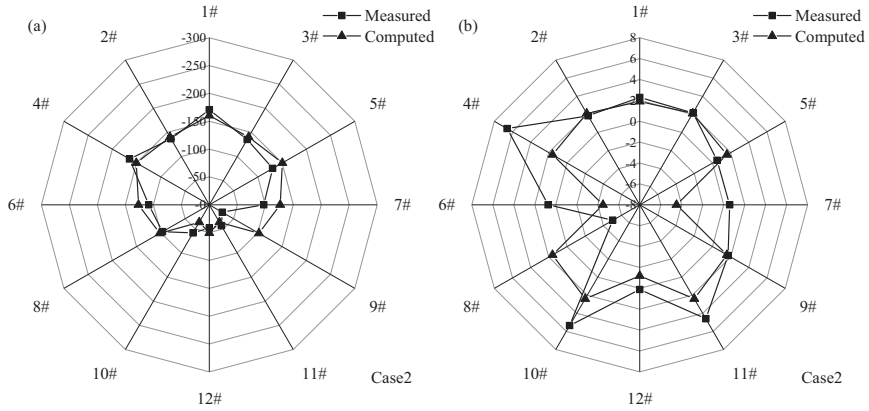


Fig. 12. Internal forces of grille steel frames (case 2): (a)Measured; (b):Computed

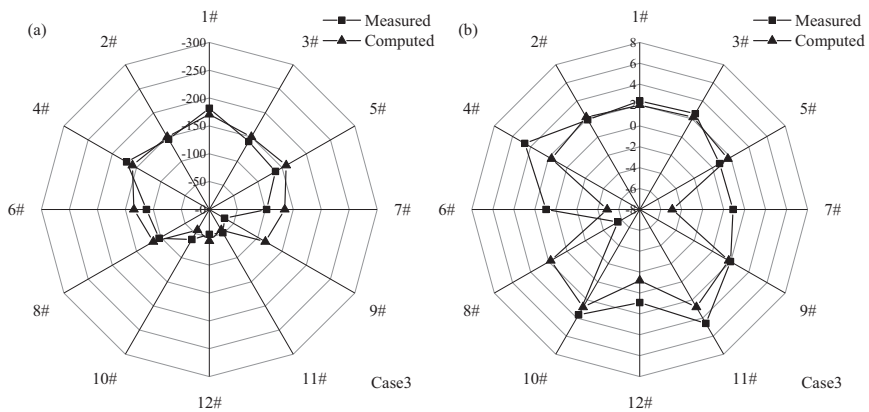


Fig. 13. Internal forces of grille steel frames (case 3): (a)Measured; (b):Computed

is about $-8 \div 8$ kN·m; the radar chart shows that the bending moment at the arch waist and side wall of the grille steel frame is large. By changing the grille type and increasing the thickness of the shotcrete layer (Case 2 and 3), the axial force of the grille steel frame at each measuring point decreases by about 20%, and the bending moment has no obvious change.

3.3. Internal force analysis of secondary lining

Combined with the field monitoring data and numerical calculation results, the distribution scatter diagram of bending moment and axial force of secondary lining vault, arch waist and side wall under three Cases is drawn when the lateral pressure coefficients are 0.8 and 1.2. In order to form a comparison with the ultimate bearing curve of secondary lining section introduced below, the absolute values of axial force and bending moment are used, as shown in Fig. 14, 15 and 16.

It can be seen from Figure 14, 15, 16 that the absolute value of axial force at the top, waist and side wall of the secondary lining is about 350–1350 kN, and the absolute value of bending moment is about 0–30 kN·m. After thinning the secondary lining, the calculation results of numerical simulation in three Cases are greater than that of field monitoring, and the numerical simulation and field monitoring results are closer when the lateral pressure coefficient is 0.8. After thinning the secondary lining, the change of the bending moment of the arch waist and the side wall is more obvious than that of the axial force. According to the field monitoring, the change of the bending moment of the side wall is up to 59%, and the change of the axial force of the vault is about 47%. When the lateral pressure coefficient is 0.8, the bending moment of each measuring point is at a low level, and the axial force distribution is more uniform than that when the lateral pressure coefficient is 1.2. Under different design conditions, the bending moment of the secondary lining is generally characterized by the distribution of “small vault, side wall and large arch waist”.

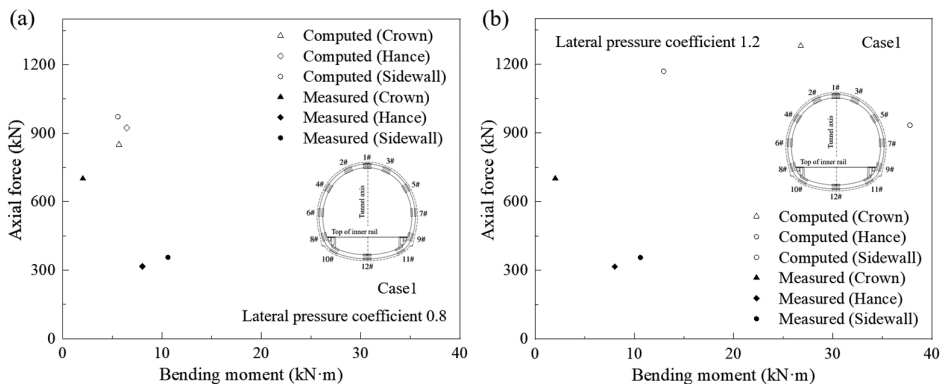


Fig. 14. Comparison of monitoring and calculation values of internal force of lining section of Tunnel (Case 1): (a) lateral pressure coefficient 0.8; (b) lateral pressure coefficient 1.2

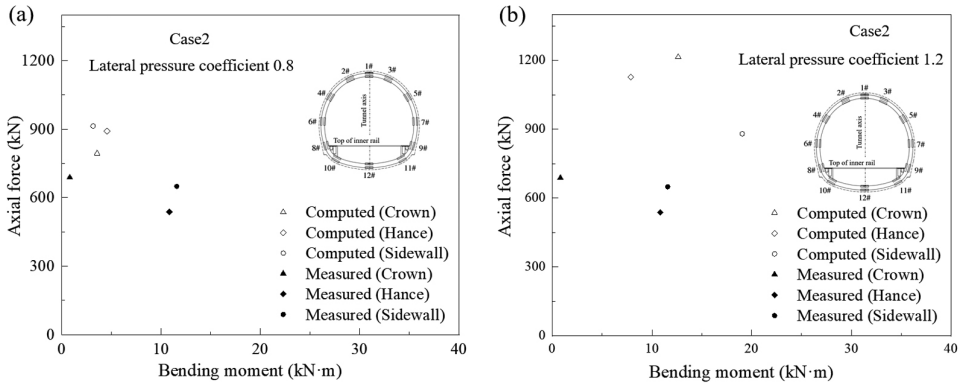


Fig. 15. Comparison of monitoring and calculation values of internal force of lining section of Tunnel (Case 2): (a) lateral pressure coefficient 0.8; (b) lateral pressure coefficient 1.2

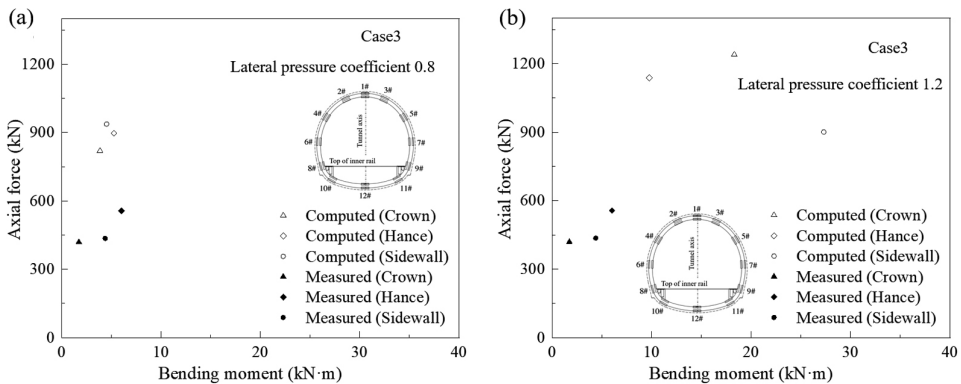


Fig. 16. Comparison of monitoring and calculation values of internal force of lining section of Tunnel (Case 3): (a) lateral pressure coefficient 0.8; (b) lateral pressure coefficient 1.2

4. Safety evaluation method of secondary lining

4.1. Ultimate bearing capacity curve of secondary lining section ($M-N$ curve)

The current tunnel specification in China uses the checking method of reinforced concrete structure as eccentric compression member to evaluate its safety. Firstly, the eccentric type of the section is determined by calculating the height x of the compression zone of the section, and the section is divided into large eccentric and small eccentric. The specific safety checking process is as follows:

1. When the lining section is under large eccentric compression ($x > 0.55h_0$, h_0 is the effective height of the section), the section safety checking formula (4.1) and (4.2) are calculated:

$$(4.1) \quad KN \leq R_w bx + R_g (A_g - A'_g)$$

$$(4.2) \quad KNe \leq R_w bx(h_0 - x/2) + R_g A'_g (h_0 - a')a,$$

where K is the safety factor; R_w is the standard value of concrete bending ultimate strength; R_g is the standard value for calculating the tensile or compressive strength of steel bars; A_g and A'_g are the sectional area of tensile and compressive steel bars, respectively. a and a' are the distance from the center of gravity of the tensile and compressive steel bars to the nearest edge of the section, respectively; e and e' are the distance between the axial force acting points of the center of gravity of the tension bar and the compression bar respectively; b is the width of section; h is the thickness of the section.

2. When the lining section is under small eccentric compression, the section safety checking formula (4.3) Calculation:

$$(4.3) \quad KNe \leq 0.5R_a bh_0^2 + R_g A'_g (h_0 - a')$$

where R_a for concrete tensile or compressive strength calculation standard value.

From the above calculation formula, it can be obtained that the main factors affecting the ultimate bearing capacity of the secondary lining section are the material parameters and geometric dimensions of the secondary lining itself, while the external load on the secondary lining has no effect on the ultimate bearing capacity of the secondary lining section.

In order to intuitively evaluate the safety of lining, the relationship between bending moment M and axial force N is derived by combining the section safety checking formula of tunnel specification and the geometric parameters of tunnel lining section, namely the ultimate bearing capacity curve of lining section. Fig. 17 shows the ultimate bearing capacity curve ($M-N$ curve) of the secondary lining section under three Cases of the tunnel. If the internal force of the secondary lining section is located inside the ultimate bearing capacity curve of the secondary lining, the section is safe, and vice versa.

Figure 17 shows that the ultimate bearing capacity curve of the secondary lining section is divided into two sections: the solid line section is controlled by the ultimate tensile strength of concrete and steel, and the axial force N increases with the increase of bending moment M . Under pure bending state (axial force N is 0), the maximum bending moments of the secondary lining sections under Case 1, 2 and 3 are 85 kN·m, 64 kN·m and 51 kN·m, respectively. The imaginary line segment is controlled by the ultimate compressive strength of concrete and steel bars, which is a curve. With the increase of axial force N , the bending moment M decreases gradually, and the flexural bearing capacity of the section decreases. Under the axial compression of the section (bending moment M is 0), the ultimate axial forces of the secondary lining sections under Case 1, 2 and 3 are 15642 kN, 13000 kN and 12392 kN.

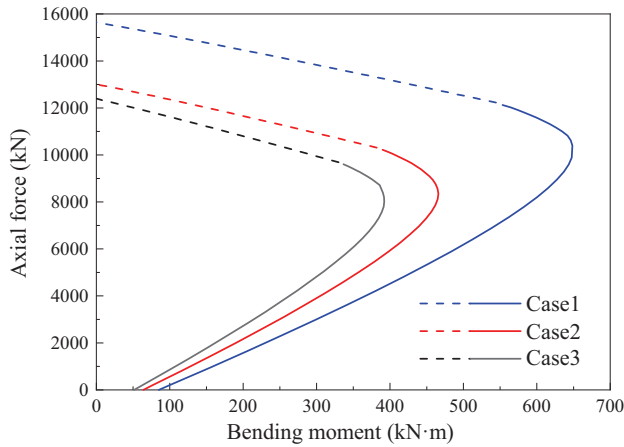


Fig. 17. Ultimate bearing capacity curve of lining section of tunnel Note: Virtual line indicates compressive failure of lining, and real line indicates tensile failure of lining.

Based on the above analysis, after the secondary lining is thinned, the maximum bending moment and axial force under condition 2 are reduced by 24.7% and 16.9% compared with the original design scheme. The maximum bending moment and axial force under condition 3 are reduced by 40% and 20.7% compared with the original design, indicating that the thinning of the secondary lining thickness has a greater impact on the bending moment than the axial force.

In order to further analyze the influence of thinned secondary lining thickness on the safety of tunnel secondary lining, the section ultimate bearing capacity curves of secondary lining under Case 1 and 2 and Case 1 and 3 are plotted in the same coordinate with the section internal force values of field monitoring and numerical simulation, as shown in Fig. 18, 19, 20 and 21.

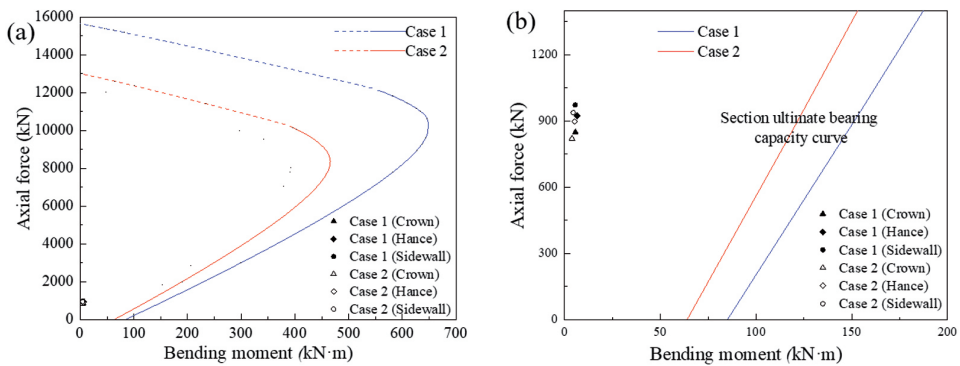


Fig. 18. Comparison between the calculated value and the limit value of lining internal force of tunnel (Case 1–Case 2) under the side pressure factor 0.8: (a) Overall view; (b) Local view

It can be seen from Figure 18, 19, 20 and 21 that the internal force of the secondary lining section is inside the ultimate bearing capacity curve of the secondary lining section

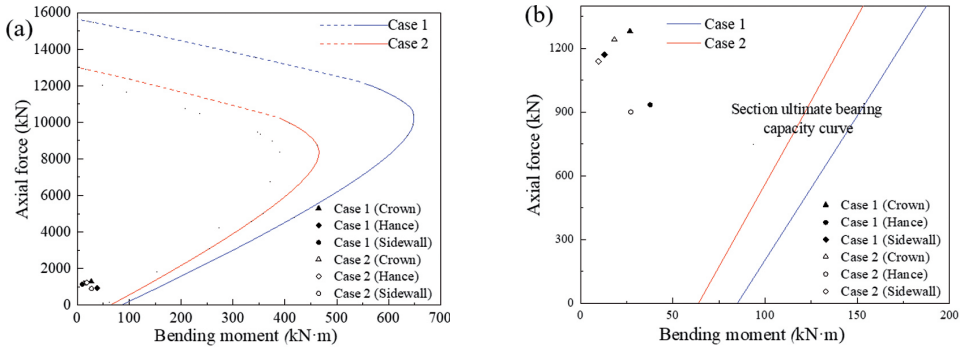


Fig. 19. Comparison between the calculated value and the limit value of lining internal force of tunnel (Case 1–Case 2) under the side pressure factor 1.2: (a) Overall view; (b) Local view

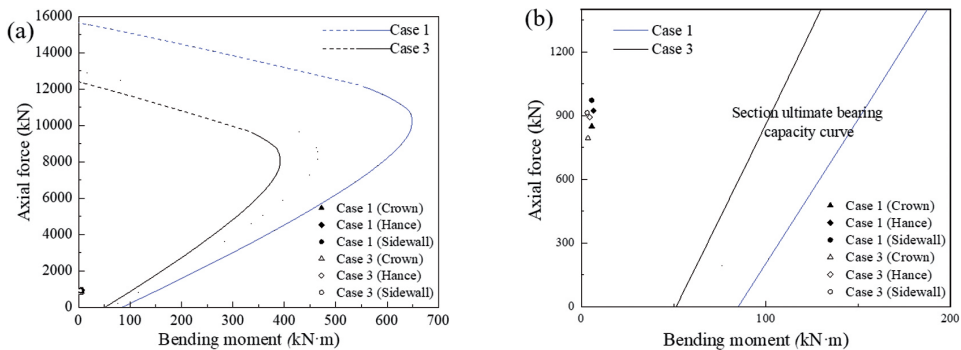


Fig. 20. Comparison between the calculated value and the limit value of lining internal force of tunnel (Case 1–Case 3) under the side pressure factor 0.8: (a) Overall view; (b) Local view

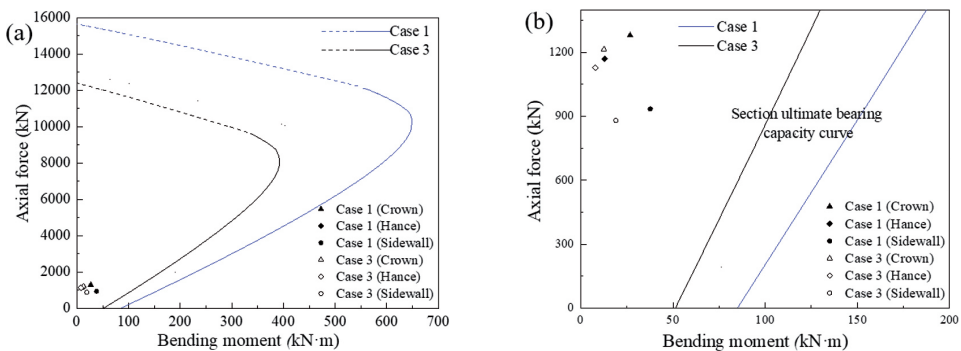


Fig. 21. Comparison between the calculated value and the limit value of lining internal force of tunnel (Case 1–Case 3) under the side pressure factor 1.2: (a) Overall view; (b) Local view

under the action of surrounding rock pressure, and is far from the ultimate bearing capacity curve of the secondary lining, which indicates that the secondary lining has a high safety reserve in this state, that is, under the condition of constant axial force, the secondary lining has a strong ability to withstand additional bending moment. At the same time, when the lateral pressure coefficient is 1.2, the internal force at each point on the secondary lining section is closer to the ultimate bearing capacity curve of the lining section, indicating that when the lateral pressure coefficient is 0.8, the stress condition of the secondary lining of the tunnel is better.

4.2. The change of bending safety factor after second lining optimization

Tunnel lining is a kind of eccentric compression structure. Under the action of bending moment, the main component of tunnel lining concrete is more likely to crack and destroy. Therefore, the bending safety of tunnel lining should be further quantitatively evaluated. According to the definition of bending safety factor in current codes, the calculation formula is as follows (4.4).

$$(4.4) \quad K_M = \frac{M_u}{M}$$

where K_M is the bending safety factor of the section; M_u is the ultimate bending moment corresponding to the axial force of lining section; M is the bending moment value of lining section

In order to quantify the influence of thinned secondary lining thickness on the safety of tunnel secondary lining, according to the ultimate bearing capacity curve of lining section and the internal force value of section monitored on site, the bending safety factor K_M of secondary lining is calculated according to formula (4.1). The results are shown in Table 3.

Table 3. Calculation table of bending safety factor under test condition

Case	Initial support				Secondary lining		Calculation of safety factor
	C25 shotcrete		Steel truss		Arch wall	Inverted arch	
	Site	Thickness (cm)	Site	Model / spacing	Thickness (cm)	Thickness (cm)	
Case 1	Whole ring	22	Whole ring	H150/1.0 m	45	50	4.1
Case 2	Whole ring	25	Whole ring	H180/1.0 m	35	45	4.5
Case 3	Whole ring	25	Whole ring	H180/1.0 m	40	35	5.3

Note: When the bending safety factor is less than 1, the lining section cracks

It can be seen from Table 3 that the bending safety factor of the original design condition is greater than 4, indicating that the original design condition is in line with the safety requirements of China's norms. After thinning the second lining, the bending safety factors of Case 2 and 3 are 4.5 and 5.3, respectively, which are larger than the original design conditions. It shows that the appropriate thinning of the second lining thickness (5–15 cm) on the basis of the original design is beneficial to improve the bending and cracking resistance of concrete.

5. Conclusions

1. Combined with numerical simulation and field monitoring, the optimal design parameters are obtained by changing the design optimization conditions of lining section parameters and taking the displacement and internal force of lining as reference: the thickness of the shotcrete layer was 25 cm, the thickness of the arch wall was 40 cm and the thickness of the inverted arch was 35 cm.
2. After the construction of tunnel is completed, the displacement value of vault settlement is significantly greater than that of inner space convergence. Compared with the original design condition, the vault settlement displacement of condition 2 and 3 is reduced by 47% and 39% respectively, and the convergence displacement of inner space is reduced by 19% and 22%.
3. The axial force of the grid steel frame is generally characterized by the distribution characteristics of "large arch, second side wall, and small invert"; the bending moment of the grille steel frame has lateral bending difference, and the bending moment at the arch waist and side wall is relatively large. After changing the grille type and increasing the thickness of shotcrete, the axial force decreases by about 10%, and the bending moment has no obvious change.
4. Compared with the original design condition, the maximum bending moment of the secondary lining section under condition 2 and 3 decreased by 24.7% and 40% respectively, and the axial force decreased by 16.9% and 20.7% respectively; after thinning the second lining, the internal force of the second and third linings decreased, especially the bending moment at the arch waist and side wall, which decreased by 59%, which was greater than the decrease of the ultimate bearing internal force of the lining section.
5. When the lateral pressure coefficient is 0.8, the calculated results are in good agreement with the monitoring values. According to field monitoring, after thinning the secondary lining, the axial force of vault decreased by 47%, and the bending moment of sidewall decreased by 59%. When the lateral pressure coefficient is 0.8, the axial force distribution of each measuring point is more uniform than that when the lateral pressure coefficient is 1.2, and the bending moment is at a relatively low level.

In this paper, the stress state of composite lining structure during construction is mainly considered. However, for heavy haul railway tunnels, the study on the variation law of the safety of initial support and secondary lining with time during tunnel operation and the

attenuation mechanism of structural safety reserve coefficient are very important for the design life of tunnels.

Acknowledgements

This work was funded by the Key Laboratory Project of Concrete Structure Safety and Durability in Shaanxi Province under Grant Nos. SZ02105, the Jingzhou Science and Technology Plan Project under Grant Nos. 2020AC15, the Young and Middle-aged Teacher Education Research Project in Fujian Province under Grant Nos. JAT210766 and the Nanping Natural Science Fund Co-funded Project in 2019 under Grant Nos. 2019J12. The authors are grateful for the great support awarded.

References

- [1] G. Sauer, V. Gall, E. Bauer, "Design of tunnel concrete linings using limit capacity cures", presented at 8th International Conference on Computer Methods and Advances in Geomechanics, 22–28 May 1994.
- [2] T. Kasper, C. Edvardsen, G. Wittneben, et al., "Lining design for the district heating tunnel in Copenhagen with steel fibre reinforced concrete segments", *Tunnelling and Underground Space Technology*, 2008, vol. 23, no. 5, pp. 574–587; DOI: [10.1016/j.tust.2007.11.001](https://doi.org/10.1016/j.tust.2007.11.001).
- [3] Y. Qiu, K. Feng, C. He, L. Zhang, et al., "Investigation of the ultimate bearing capacity of a staggered assembly segmental lining for an urban gas transmission tunnel", *Sustainable Cities and Society*, 2019, vol. 48, pp. 1–13; DOI: [10.1016/j.scs.2019.101551](https://doi.org/10.1016/j.scs.2019.101551).
- [4] A.D. Mai, M.N. Sheikh, M.N.S. Hadi, "Failure envelopes of square and circularized RC columns discretely confined with CFRP", *Construction and Building Materials*, 2020, vol. 261, pp. 1–11; DOI: [10.1016/j.conbuildmat.2020.119937](https://doi.org/10.1016/j.conbuildmat.2020.119937).
- [5] W.B. Ma, J.F. Chai, Z. Han, et al., "Research on design parameters and fatigue life of tunnel bottom structure of single-track ballasted heavy-haul railway tunnel with 40-ton axle load", *Mathematical Problems in Engineering*, 2020, vol. 2020, pp. 1–9; DOI: [10.1155/2020/3181480](https://doi.org/10.1155/2020/3181480).
- [6] J. Pengfei, X. Zhang, X. Li, et al., "Optimization analysis of construction scheme for large-span highway tunnel under complex conditons", *Archives of Civil Engineering*, 2018, vol. 64, no. 4/I, pp. 55–68; DOI: [10.2478/ace-2018-0044](https://doi.org/10.2478/ace-2018-0044).
- [7] A. Vanuvamalai, K.P. Jaya, "Design analysis of an underground tunnel in tamilnadu", *Archives of Civil Engineering*, 2018, vol. 64, no. 1, pp. 21–39; DOI: [10.2478/ace-2018-0002](https://doi.org/10.2478/ace-2018-0002).
- [8] M. Ghaffari, S. Mahdevari, "The effect of tunnel geometry and geomechanical parameters of host rock on tunnel displacement profile", *Geotechnical and Geological Engineering*, 2022, vol. 40, pp. 2799–2809; DOI: [10.1007/s10706-022-02063-3](https://doi.org/10.1007/s10706-022-02063-3).
- [9] K. Yertutanol, H. Akgun, E. Sopaci, "Displacement monitoring, displacement verification and stability assessment of the critical sections of the Konak tunnel, İzmir, Turkey", *Tunnelling and Underground Space Technology*, 2020, vol. 101, art. ID 103357; DOI: [10.1016/j.tust.2020.103357](https://doi.org/10.1016/j.tust.2020.103357).
- [10] S.M. Gao, J.P. Chen, C.Q. Zuo, et al., "Structure optimization for the support system in soft rock tunnel based on numerical analysis and field monitoring", *Geotechnical and Geological Engineering*, 2016, vol. 34, pp. 1089–1099; DOI: [10.1007/s10706-016-0029-3](https://doi.org/10.1007/s10706-016-0029-3).
- [11] Q. Jiang, S.G. Song, T. Li, et al., "Study on surrounding rock stability of small clear-distance twin highway tunnel with eight lanes", *Geotechnical and Geological Engineering*, 2019 vol. 37, pp. 593–598; DOI: [10.1007/s10706-018-0629-1](https://doi.org/10.1007/s10706-018-0629-1).
- [12] S.O. Choi, H-S. Shin, "Stability analysis of a tunnel excavated in a weak rock mass and the optimal supporting system design", *International Journal of Rock Mechanics and Mining Sciences*, 2004, vol. 41, pp. 876–881; DOI: [10.1016/j.ijrmms.2004.03.151](https://doi.org/10.1016/j.ijrmms.2004.03.151).

- [13] H.H.A. Rahim, M. Enieb, A.A. Khalil, et al., “Twin tunnel configuration for Greater Cairo metro line No. 4”, *Computer and Geotechnics*, 2015, vol. 68, pp. 66–77; DOI: [10.1016/j.compgeo.2015.03.015](https://doi.org/10.1016/j.compgeo.2015.03.015).
- [14] H.F. Qu, H.H. Zhu, C.Z. Huang, et al., “Study on selection of section-steel and grid-steel in primary support system of tunnel”, *Chinese Journal of Underground Space and Engineering*, 2007, vol. 3, no. 2, pp. 258–262; DOI: [10.3969/j.issn.1673-0836.2007.02.015](https://doi.org/10.3969/j.issn.1673-0836.2007.02.015).
- [15] J. Wang, E. Li, L. Chen, et al., “Measurement and analysis of the internal displacement and spatial effect due to tunnel excavation in hard rock”, *Tunnelling and Underground Space Technology*, 2019, vol. 84, pp. 151–165; DOI: [10.1016/j.tust.2018.11.001](https://doi.org/10.1016/j.tust.2018.11.001).
- [16] G.S. Zeng, H.N. Wang, M.J. Jiang, et al., “Analytical solution of displacement and stress induced by the sequential excavation of noncircular tunnels in viscoelastic rock”, *International Journal of Rock Mechanics and Mining Sciences*, 2020, vol. 134; DOI: [10.1016/j.ijrmms.2020.104429](https://doi.org/10.1016/j.ijrmms.2020.104429).
- [17] J.S. Zhang, Y.Z. Qi, “Research on the intelligent positioning method of tunnel excavation face”, *Archives of Civil Engineering*, 2022, vol. 68, no. 1, pp. 431–441; DOI: [10.24425/ace.2022.140178](https://doi.org/10.24425/ace.2022.140178).
- [18] G. Leonardi, R. Palamara, F. Suraci, “3D Finite element model of a blast load in a tunnel”, *Archives of Civil Engineering*, 2021, vol. 67, no 4, pp. 91–105; DOI: [10.24425/ace.2021.138488](https://doi.org/10.24425/ace.2021.138488).

Received: 2022-05-17, Revised: 2022-06-28